

<https://helda.helsinki.fi>

Energy loss in low energy nuclear recoils in dark matter detector materials

Sassi, Sebastian

2022-09-15

Sassi , S , Heikinheimo , M , Tuominen , K , Kuronen , A , Byggmästar , J , Nordlund , K & Mirabolfathi , N 2022 , ' Energy loss in low energy nuclear recoils in dark matter detector materials ' , Physical Review D , vol. 106 , no. 6 , 063012 . <https://doi.org/10.1103/PhysRevD.106.063012>

<http://hdl.handle.net/10138/350835>

<https://doi.org/10.1103/PhysRevD.106.063012>

cc_by

publishedVersion

Downloaded from Helda, University of Helsinki institutional repository.

This is an electronic reprint of the original article.

This reprint may differ from the original in pagination and typographic detail.

Please cite the original version.

Energy loss in low energy nuclear recoils in dark matter detector materials

Sebastian Sassi,^{*} Matti Heikinheimo[†], Kimmo Tuominen[‡], Antti Kuronen[§],
Jesper Byggmästar^{||} and Kai Nordlund[¶]

*Department of Physics, University of Helsinki and Helsinki Institute of Physics,
P.O. Box 64, FI-00014 Helsinki, Finland*

Nader Mirabolfathi^{**}

*Department of Physics and Astronomy and the Mitchell Institute for Fundamental Physics and Astronomy,
Texas A&M University, College Station, Texas 77843, USA*



(Received 20 June 2022; accepted 23 August 2022; published 15 September 2022)

Recent progress in phonon-mediated detectors with eV-scale nuclear recoil energy sensitivity requires an understanding of the effect of the crystalline defects on the energy spectrum expected from dark matter or neutrino coherent scattering. We perform molecular dynamics simulations to determine the amount of energy stored in the lattice defects as a function of the recoil direction and energy. This energy cannot be observed in the phonon measurement, thus affecting the observed energy spectrum compared to the underlying true recoil energy spectrum. We describe this effect for multiple commonly used detector materials and demonstrate how the predicted energy spectrum from dark matter scattering is modified.

DOI: [10.1103/PhysRevD.106.063012](https://doi.org/10.1103/PhysRevD.106.063012)

I. INTRODUCTION

The cosmological and astronomical evidence for the existence of dark matter (DM), which comprises the vast majority of the mass content of the Universe, is abundant [1,2]. Among dark matter candidates, many models predict particles that can elastically scatter off the electrons or nuclei, releasing a measurable energy in the detectors. Because of the very low energy recoils expected from the galactic DM halo, the interaction of DM particles with the detector nucleus is particularly interesting. This is because at low momentum transfers, the particles are expected to coherently interact with the nucleons in the nucleus, increasing the cross section of the interaction by A^2 , where A is the atomic number of the target material. In the past, attempts of such direct detection of DM scattering on nuclei have mostly focused on the DM mass range $m_{\text{DM}} \gtrsim 1$ GeV (we use natural units $\hbar = c = 1$), and the most stringent

exclusion limits for DM nucleon scattering have been obtained for $m_{\text{DM}} \gtrsim 10$ GeV [3].

Very low threshold detectors are needed to measure the small energies from DM interactions with nuclei for DM masses in the sub-GeV range. Recently, several groups [4–8] have developed detectors with detection thresholds in the $\mathcal{O}(10)$ eV recoil energy range. Among those technologies, the phonon-mediated detectors are particularly interesting because their energy measurement indicates the true recoil energy. This is in contrast to the ionization or scintillation detectors wherein the true recoil energy should be corrected for the ionization or scintillation yield [9]. Currently, these experiments observe an event rate in excess of the anticipated background [10]. Until the origin of this excess is clarified, it provides an obstruction for reaching the necessary sensitivity of the experiment to a DM signal.

At recoil energies below a few hundred eV, it becomes necessary to understand the detailed response of the target material to the DM scattering. Recent developments on the theoretical description of matter effects in direct detection of light dark matter include Refs. [11–13] and the references therein. For nuclear recoils, the observed recoil spectrum in phonon-based detectors can be influenced by the creation of crystal defects in the target material: Part of the true recoil energy is stored in the defect and will not reach the phonon detector, resulting in a lower observed energy for the event. To understand and interpret the observed spectrum in terms of the physical processes responsible for the recoil events, this effect needs to be

^{*}sebastian.k.sassi@helsinki.fi

[†]matti.heikinheimo@helsinki.fi

[‡]kimmo.i.tuominen@helsinki.fi

[§]antti.kuronen@helsinki.fi

^{||}jesper.byggmastar@helsinki.fi

[¶]kai.nordlund@helsinki.fi

^{**}mirabolfathi@physics.tamu.edu

Published by the American Physical Society under the terms of the Creative Commons Attribution 4.0 International license. Further distribution of this work must maintain attribution to the author(s) and the published article's title, journal citation, and DOI. Funded by SCOAP³.

accounted for [14]. For this purpose, the energy stored in the defects must be known as a function of the recoil direction and recoil energy.

In this paper, we report the results from molecular dynamics simulations performed for multiple commonly used or proposed detector materials. These are sapphire (Al_2O_3), silicon carbide (SiC), tungsten carbide (WC), diamond (C), silicon (Si), germanium (Ge), and tungsten (W). Using these results, we then describe the resulting modifications in the expected dark matter recoil spectrum in phonon-based detectors. We have proposed a method utilizing this effect to identify the origin of the low energy excess events observed in multiple experiments in [15].

The paper is organized as follows: In Sec. II we present the setup and results of the molecular dynamics simulations. Then, in Sec. III we explain how the crystal defects affect the observed spectrum of DM recoils, emphasizing the dependence on the target material. In Sec. IV we present our conclusions and outlook for future work.

II. MOLECULAR DYNAMICS SIMULATIONS

A. Simulation setup

The molecular dynamics simulations for Al_2O_3 , SiC, WC, and W were done using the LAMMPS molecular dynamics simulator [16], while the simulations for C, Si, and Ge were done previously using the PARCAS code [17,18]. Otherwise, the principles for these simulations are the same as described below, following general principles previously used to examine threshold displacement

energies in materials [17,19,20]. The simulation parameters and potentials used for each material are listed in Table I.

The simulation region was constructed from orthogonal unit cells such that the region would have roughly the same size in each dimension and would contain $O(10^3)$ atoms. For SiC and WC, which have a hexagonal conventional unit cell, an orthogonal unit cell twice the size of the hexagonal cell was used. The boundary conditions were periodic in each direction. The simulations were done at a temperature of 40 mK. To achieve this, for each material the simulation box was first allowed to reach an equilibrium state by running it for 1 ps under temperature and pressure control at the target temperature of 40 mK under no external pressure. The final configuration of this simulation would then be used as the starting configuration of all the recoil simulations for that material. We note that in classical molecular dynamics, the quantum mechanical zero-point vibrations of atoms were not included in the description of atom motion. However, we have previously found, by comparing 40 mK results with higher temperature ones, that this does not affect the damage production probability because the recoil kinetic energies > 10 eV are several orders of magnitude higher than the meV thermal vibration energies [20].

To let kinetic energy dissipate in the recoil simulations, the simulation box was divided into two regions: an interior where the recoils would take place, and a border region under temperature control at 40 mK to dissipate thermal energy into the surroundings. The thickness of the border region was set to 6.0 angstroms in all simulations.

TABLE I. Parameters and potentials used in the simulations. The simulations for C, Si, and Ge were done previously using the PARCAS code [17,18], which employs an adaptive time step algorithm in radiation effect calculations [21].

	Al_2O_3	SiC	WC
Unit cell config.	$8 \times 5 \times 3$	$5 \times 9 \times 3$	$10 \times 6 \times 10$
Atoms per unit cell	60	16	4
Time step (ps)	0.0005	0.0005	0.00025
Simulation time (ps)	4.0	4.0	3.2
Potential	Vashishta <i>et al.</i> [22]	Gao-Weber [23]	Juslin <i>et al.</i> [24]
	C	Si	Ge
Unit cell config.	$8 \times 8 \times 8$	$8 \times 8 \times 8$	$8 \times 8 \times 8$
Atoms per unit cell	8	8	8
Time step (ps)	Adaptive	Adaptive	Adaptive
Simulation time (ps)	20.0	20.0	20.0
Potential	Erhart [25], Tersoff-Nordlund [27,28]	Stillinger-Weber [26]	Modified Stillinger-Weber [17]
	W		
Unit cell config.	$10 \times 10 \times 10$		
Atoms per unit cell	2		
Time step (ps)	0.00009		
Simulation time (ps)	4.2		
Potential	Derlet-Björkas [29,30]		

To simulate nuclear recoils over a given range of recoil energies, for each atom inside the unit cell closest to the center of the simulation box, random recoil directions were sampled uniformly on the sphere. For a given direction, for each recoil energy in the simulated range, the energy and direction would be used to set the velocity of the atom to simulate increasingly energetic recoils in the direction. The numbers of simulated directions vary for the different materials, but all the data presented here are based on $\gtrsim 1000$ recoil directions. After the velocity of the recoiling atom was set, the simulation was run for a fixed amount of time, depending on the target material, to let the system return as close to an equilibrium as viable. This time was primarily constrained by practical considerations of execution time. A sufficient simulation time was determined by running longer test simulations (> 5 ps) at different recoil energies and observing how long it took for the system's potential energy to fall to within < 1 eV of its final value. The size of the time step for each material was chosen based on similar considerations of stability of the system's energy under changes in size of the time step.

As alluded to above, the energy lost to defects was based on calculating the difference in the potential energy of the system at the start of the simulation before the recoil, and at the end of the simulation. Since the permanent energy loss in these materials should be associated with creation of at least one Frenkel pair, a consistency check was performed on the occupation numbers of each Wigner-Seitz cell (for non-Bravais lattices this is the Voronoy polyhedron surrounding each atom position [31]) in the simulation box, with occupation number differing from one, indicating a defect. Although there are numerous ways to analyze defects in crystals, this Wigner-Seitz cell/Voronoy polyhedron approach has the advantage of not involving any free parameters and not counting bond order defects that likely are metastable [17]. If no defects are found, a value of zero would be recorded for the energy loss. Otherwise, the potential energy difference at the start and end of the simulation is recorded.

B. Results

We find that there exists significant variance in the energy loss characteristics between the simulated materials. On the left-hand side of Fig. 1, the defect probabilities, defined here as the average over the sampled directions, at different recoil energies are shown. It is noteworthy that for pure elemental C, simulations were performed with two different interatomic potentials. Throughout the results, as seen in Fig. 1, it will be evident that there is little difference in defect creation and energy loss between the different potentials, giving some confidence that these results are not highly sensitive to the details of the model for interatomic forces.

In the single-element materials and in SiC, we see that the defect creation probability from nuclear recoils generally

increases steeply after the initial minimum energy threshold for defect creation is reached. Although in SiC the defect probability for C recoils increases later, the probability for both elements quickly approaches unity above recoil energies of 50 eV. In sharp contrast, in Al_2O_3 , the defect creation probability only increases gradually, with a significant likelihood of no defect creation even at recoil energies of 200 eV for both Al and O recoils, and O recoils remaining significantly less likely than Al recoils throughout the energy range. WC is an interesting case because of the large difference in masses of the W and C atoms. Here, there is a significant difference in the initial threshold for defect creation between the atoms, which is likely due to the aforementioned mass difference. Regardless of the initial difference, around 200 eV, the defect probability from both types of recoils again approaches unity.

The defect formation probability in pure W differs strongly from the other materials considered in this work. This is to be expected since densely packed elemental metals have a very strong athermal damage recombination effect [32,33]. This causes the damage production in common metals to be much less efficient than in covalently bonded materials such as Si and Ge [17]. Because of this effect, both the defect formation probability and permanent energy loss are much lower than in the nonmetallic materials considered in this study (Fig. 1).

The behavior of the defect formation probability as a function of recoil energy could, in principle, result from directional variation in the initial defect creation threshold or recombination of defects moments after their creation. Indeed, we find both effects at play. While there is directional variation in the materials, there is significant variation between materials in how likely defects are to form after the threshold recoil energy for defect creation has been exceeded. Figure 2 shows defect creation and recombination trends for an illustrative sample of directions for each material, where the recoil energies at which defects were created have been colored. The samples have been picked from the full simulated sample of random directions to showcase typical behavior in the given material. Here it is seen that for elemental C, as well as SiC, at recoil energies above 100 eV, defects almost always form. Si and Ge display a little more recombination, which is reflected in the slower increase of the defect creation probability. For Al_2O_3 in turn, especially in O recoils, defects are highly likely to recombine even at the maximum simulated recoil energies of 200 eV.

It is evident that in a material like Al_2O_3 with significant recombination, the initial defect creation threshold for a given direction can be difficult to determine. Indeed, some of the simulated directions not shown here show no defects in the whole simulated recoil energy range, but it is clearly wrong to conclude that 200 eV of recoil energy is not sufficient to create defects. Even in the less extreme cases, significant recombination obscures the directional variation

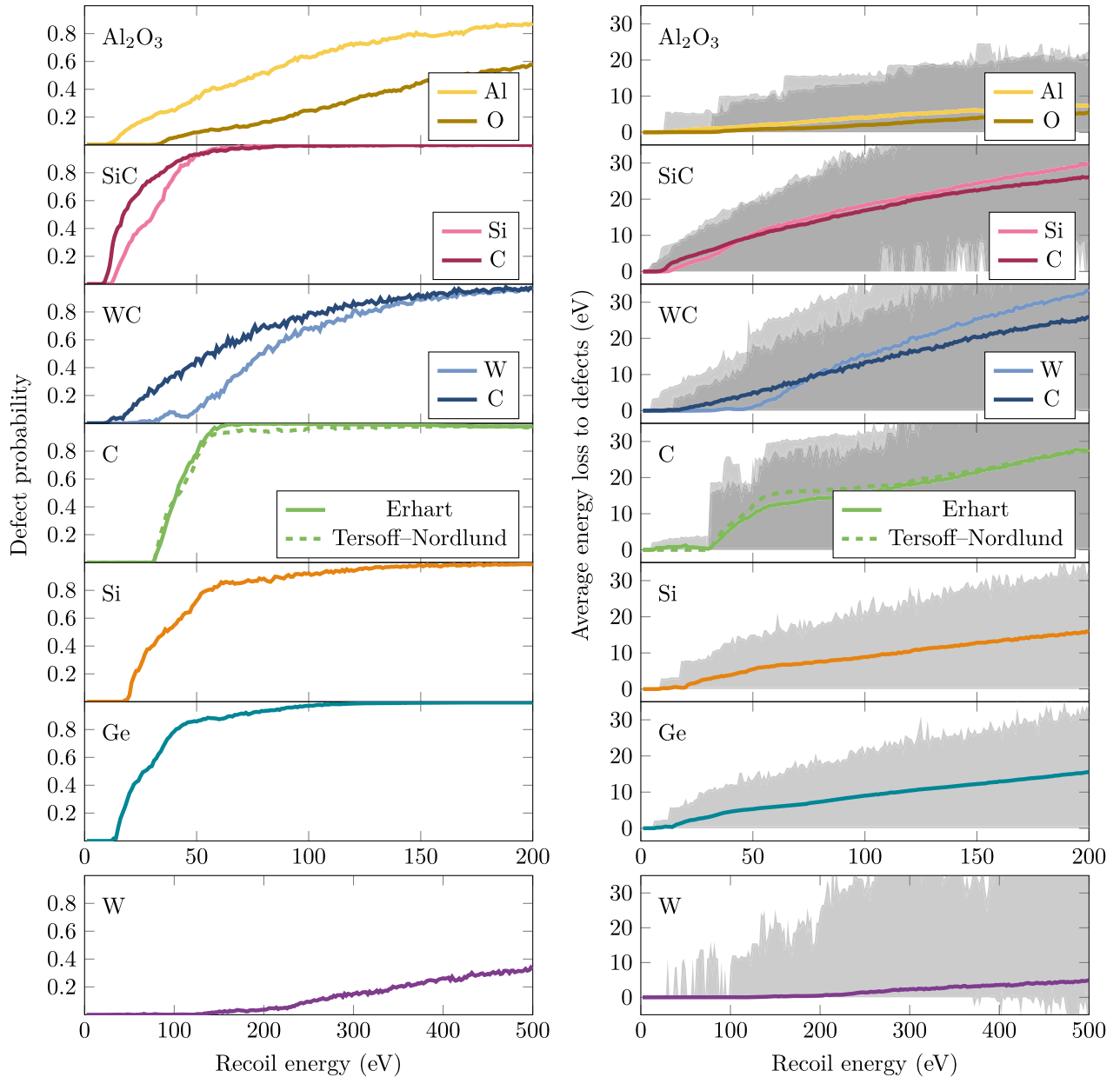


FIG. 1. Left: probability of defect creation from a nuclear recoil as a function of recoil energy in the simulated materials. Right: average energy loss in the materials (solid lines) and range of energy loss (gray bands). The minimum defect creation energies for each material are listed in Table II. Figures 3 and 4 show the spread of energy loss in more detail.

in the defect creation threshold energy, making it potentially seem more significant than it actually is. Therefore, for the materials with a significant degree of recombination, these data may not be useful for showcasing directional variation in the defect creation threshold.

On the right-hand side of Fig. 1, the energy loss averaged over recoil direction for each material is shown as a function of recoil energy. The trends here largely reflect the trends seen in defect creation probability on the left-hand side of Fig. 1, although here the fact that the amount of defects, and therefore the energy lost to defects, also increases as a function of recoil energy linearizes the trends. Hence, Al₂O₃

generally has very little energy loss, and because the average defect creation threshold is less pronounced, so is the threshold for energy loss. The average energy loss shows the effect of the different amounts of energy stored in defects in different materials. Although SiC and elemental C, Si, and Ge behave roughly similarly in the defect creation probability, Si and Ge have significantly lower average energy loss due to defects in the latter materials generally storing less energy. Here a minor difference is also seen between the two different potentials for elemental C. In WC, we see the disparity between the W and C recoils pronounced, and while the threshold in energy loss for C is

TABLE II. Minimum defect creation threshold energies $E_{t,\min}$ for the simulated materials.

Material	Recoil atom	$E_{t,\min}$ (eV)
Al ₂ O ₃	Al	11
Al ₂ O ₃	O	31
SiC	Si	11
SiC	C	9
WC	W	18
WC	C	9
C-Erhart		31
C-TN		31
Si		18
Ge		13
W		30

damped, showing a very linear increase, W retains a more pronounced threshold. It is interesting to note in the context of WC that if the scattering is coherent (and so the cross section of the recoil process is proportional to the squared mass number A^2), then the rate of C recoils will be very small compared to the rate of W recoils. Consequently, a recoil experiment measuring energy loss should mainly see the energy loss curve of W recoils.

Figures 3 and 4 show a more detailed picture of the energy loss. Here the probability density of energy loss is plotted at various recoil energies (i.e., adding the probabilities over the energy loss for a given recoil energy gives unity). These figures show the above-mentioned differences in energy stored in defects. For elemental C, at low recoil energies, most of the generated defect configurations store around 10–15 eV of energy with nothing below that, whereas for Si, Ge, and SiC the lowest amount of energy stored is around 5 eV. As the recoil energy increases, the distribution of energy loss tends to spread out. This spreading out is particularly pronounced in the covalently bonded materials SiC and WC, which have fairly complex and open crystal structures. In such materials, there are many possibilities for different metastable disordered defect configurations, which lead to a large variation in the energy loss to defects. Conversely, the very hard C in the diamond structure also has high resistance to radiation damage and hence less variation. The small variation in Al₂O₃ is likely due to the strong ionic character in its bonding, reducing the number of possible defect configurations (the Coulombic forces between like charges essentially hinder atoms of the same type to remain close to each other). In W, there is also some spread, but note that

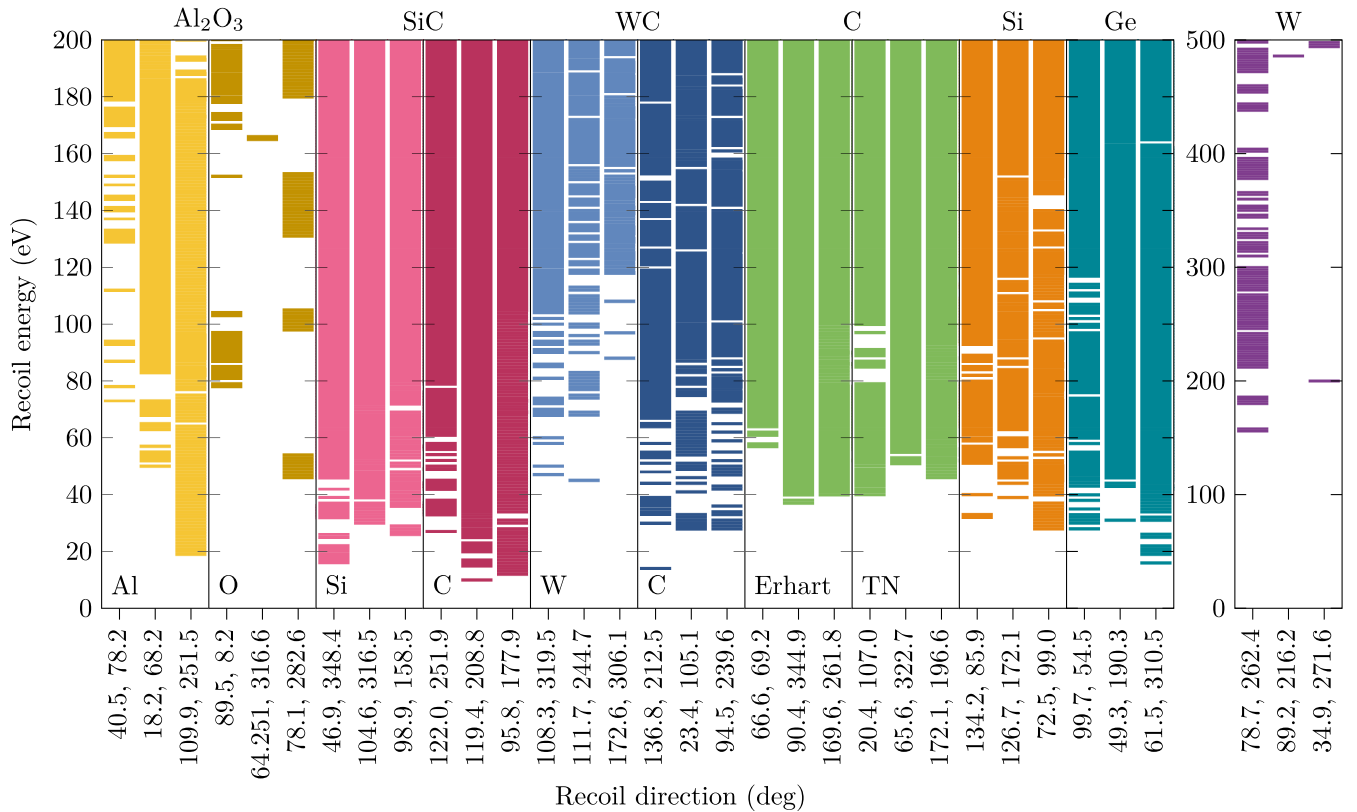


FIG. 2. Illustrative sample of directions demonstrating typical defect creation in the simulated materials. Energies for which a defect was created have been colored in, while energies that produced no defects have been left blank. The direction of each recoil is shown below in degrees, with the first angle being the colatitude and the second the azimuthal angle. Note that the choice of directions has no special significance.

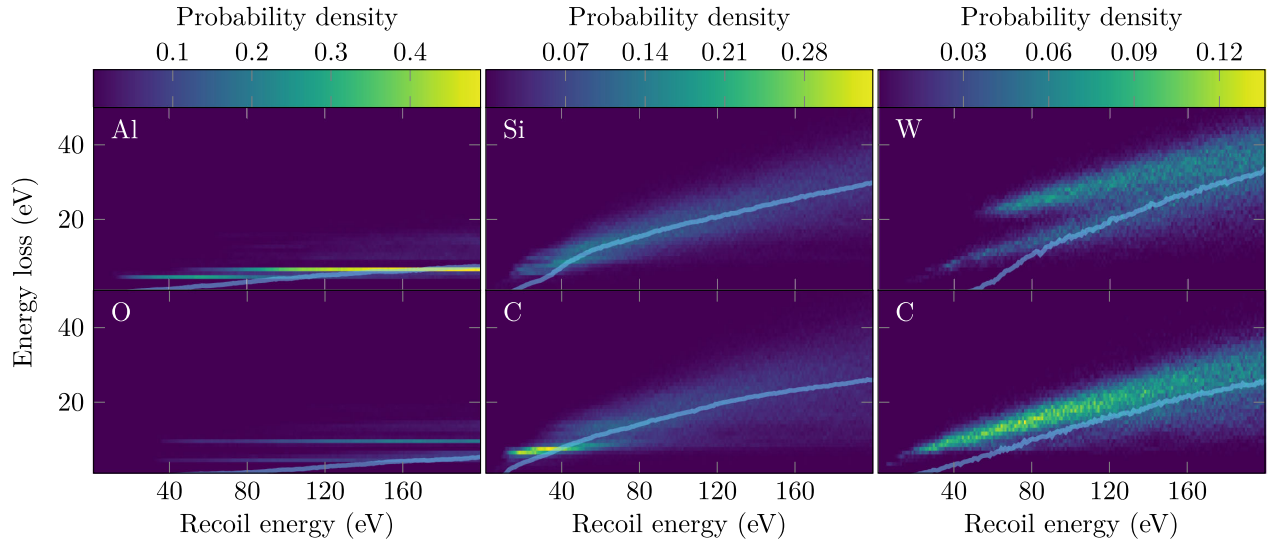


FIG. 3. Probability distribution of energy loss parametrized by recoil energy for Al_2O_3 , SiC, and WC. The energy loss has been binned with 1 eV intervals. The solid line shows the average energy loss. Note that the 0 eV bin (no defects) is included in the probability density but has been left off the figure to focus on the distribution of energy loss when defects are produced. As a consequence, the average energy loss trails below the bands in the figure when the probability of defect production is low.

this spread is at much higher energies than in the other materials due to the recombination effect mentioned above. This spread can be understood in terms of occasional formation of extended defects with complex geometry [34,35].

III. RECOIL SPECTRUM FOR DM

Because the energy loss depends strongly on the recoil direction, we first compute the expected DM-nucleus recoil event rate as a function of direction and energy, given by

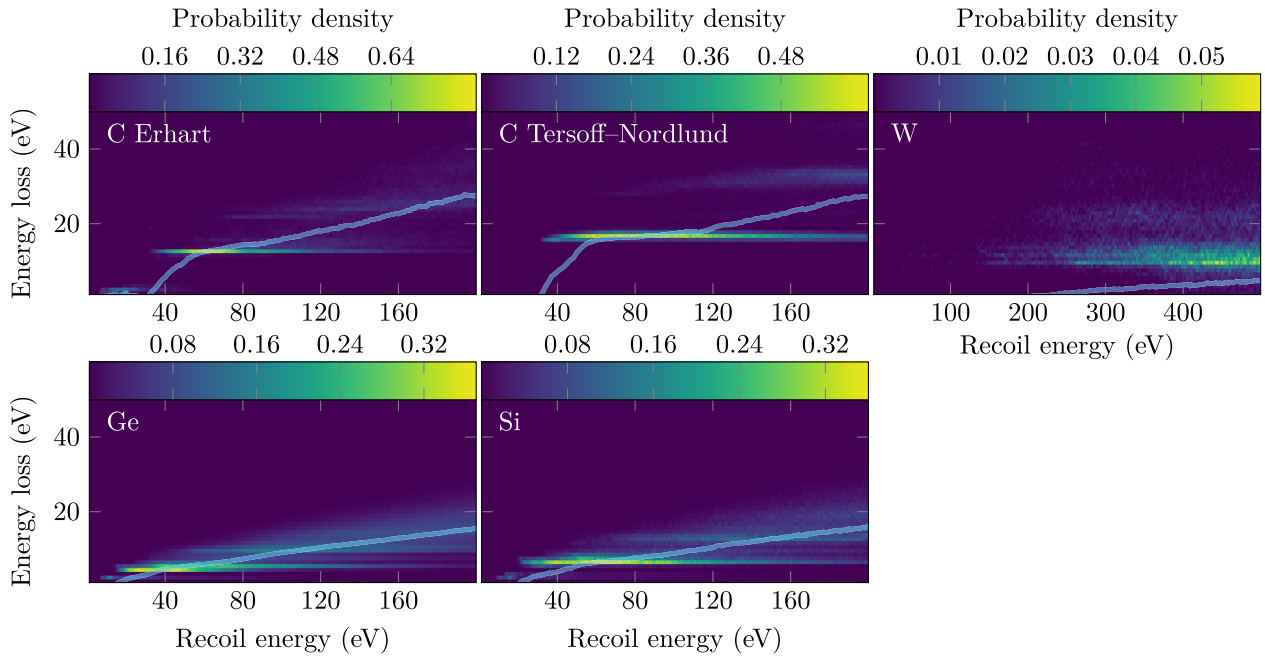


FIG. 4. Probability distribution of energy loss parametrized by recoil energy for C with Erhart and Tersoff-Nordlund potentials, Ge, Si, and W. See caption of Fig. 3 for details.

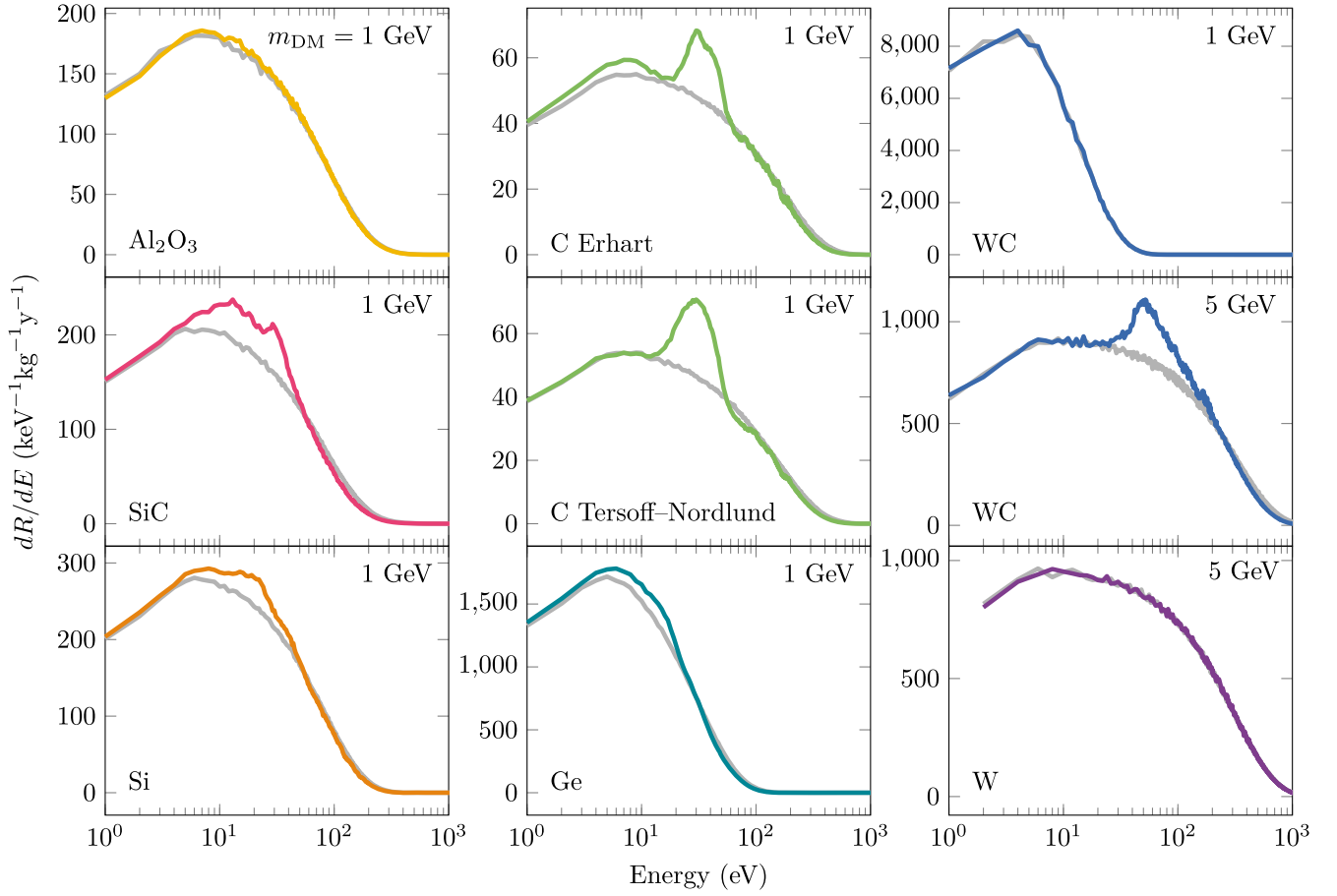


FIG. 5. Impact of energy loss on the DM differential event rate dR/dE_{rec} . For each material the grey line is the rate in that material without energy loss, and the colored line is the rate after energy loss. The dark matter mass is shown in the top right corner.

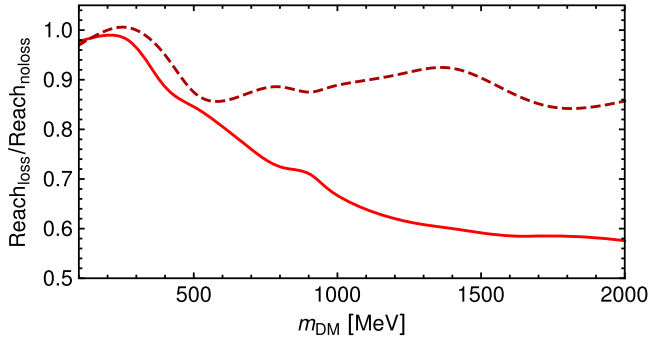


FIG. 6. Gain in the reach of a diamond detector due to the energy loss effect against an electron recoil background with a flat energy spectrum. The dashed line shows the ratio of the discovery reach (the lowest observable SI cross section) after the energy loss effect to the reach without the effect for a 1 kg year experiment. The solid line shows the same for a 100 kg year experiment.

$$\frac{dR}{dEd\Omega_q} = \frac{\rho_0 A^2 F(E) \sigma_{\text{DMn}}}{4\pi m_{\text{DM}} \mu_{\text{DMn}}^2} \hat{f}(v_{\min}, \hat{\mathbf{q}}), \quad (1)$$

where $\mu_{\text{DMn}} = m_{\text{DM}} m_n / (m_{\text{DM}} + m_n)$ is the reduced mass of the DM-nucleon system, A is the mass number of the target

nucleus, $F(E)$ is the nuclear form factor, and ρ_0 is the local DM density. For simplicity, we have assumed a spin-independent interaction, characterized by the DM-nucleon scattering cross section σ_{DMn} . The dependence on the recoil direction, parametrized by the recoil momentum unit vector $\hat{\mathbf{q}}$, is in the Radon transform of the DM velocity distribution \hat{f} defined as

$$\hat{f}(v_{\min}, \hat{\mathbf{q}}) = \int f(v) \delta(\mathbf{v} \cdot \hat{\mathbf{q}} - v_{\min}) d^3 v, \quad (2)$$

where $v_{\min} = \sqrt{m_N E / (2\mu_{\text{DMN}}^2)}$ is the minimum velocity of the DM particle in the lab frame required to excite a nuclear recoil with energy E for a nucleus with a nuclear mass m_N , and μ_{DMN} is the DM-nucleus reduced mass. For simplicity, we assume here the standard halo model for the velocity distribution of DM,

$$f_{\text{SHM}}(v) = \frac{1}{N_{\text{esc}}} \frac{1}{(2\pi\sigma_v^2)^{\frac{3}{2}}} e^{-\frac{v^2}{2\sigma_v^2}} \Theta(v_{\text{esc}} - v), \quad (3)$$

where σ_v is the velocity dispersion and v_{esc} is the escape velocity. The analytical formulas of the Radon transform

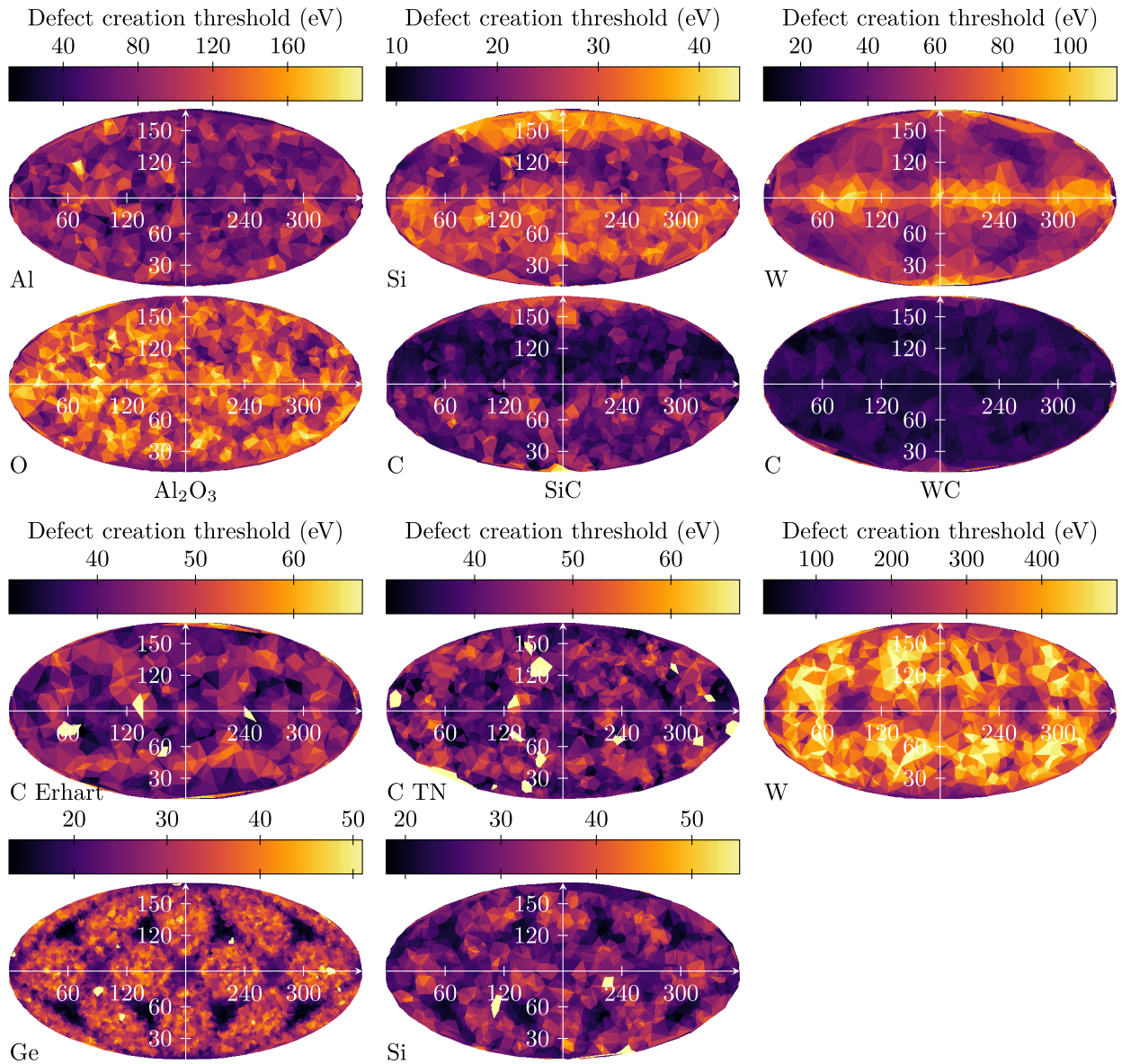


FIG. 7. Mollweide projection of the angular distribution of defect creation thresholds in the materials. The top six plots show the compound materials for each recoil atom. The bottom five plots show the single-element materials. Directions where no defect was produced at any energy have been mapped to the highest simulated recoil energy. Because of this, in order to show the directional anisotropy, the maximum value of the color map is not the highest threshold energy, but it has been chosen to be the 99th percentile threshold energy. It is also worth noting that the threshold energy here is merely the lowest energy at which we observed a defect in our simulations. Because of the probabilistic nature of defect production around the threshold, these values may not correspond to the true threshold in the sense of, e.g., the recoil energy above which 50% of recoils lead to defects. Therefore, while in the materials where recombination of defects is rare (such as Ge) the distribution is likely fairly accurate, in materials with lots of recombination such as Al_2O_3 there is likely a significant amount of noise.

\hat{f}_{SHM} shifted to the laboratory frame and integrated over recoil energy can be found in [36].

To obtain the observed recoil spectrum in a phonon measurement after the energy loss, we perform a simulation as follows: First, the recoil direction surface (unit sphere) is divided into solid angle bins corresponding to the directions for which the MD simulations were performed, as described

in Sec. II. Each solid angle bin is then further divided into energy bins using 1 eV intervals, for which we find the DM event rate using (1). This procedure results in a binned underlying event rate, reflecting the energy deposited by the DM scattering events. We then sample this underlying event rate, and for each sampled event with recoil energy E_r and recoil direction $\hat{\mathbf{q}}$, we find the observed energy as

$$E_{\text{obs}} = E_r - E_{\text{loss}}(E_r, \hat{\mathbf{q}}) + E_\sigma, \quad (4)$$

where $E_{\text{loss}}(E_r, \hat{\mathbf{q}})$ is obtained from the MD simulations and E_σ is a random number drawn from a Gaussian distribution with zero mean and standard deviation σ representing the energy resolution of the detector, for which we use $\sigma = 3$ eV. The result after this sampling is the binned observed recoil rate, which we then sum over the solid angle bins as the detector is not capable of observing the recoil direction, to obtain the observed recoil spectrum dR/dE_{obs} .

The resulting recoil spectrum is shown in Fig. 5, for a 1 GeV DM particle (and 5 GeV for WC and W) in the simulated detector materials, normalized to DM-nucleon cross section $\sigma_{\text{DMn}} = 10^{-42}$ cm². The colored curves show the result with the computed energy loss E_{loss} , while the gray curves correspond to the case without the energy loss effect, i.e., setting $E_{\text{loss}} = 0$ in Eq. (4).

As seen from the figure, the sharp defect creation threshold in diamond results in a prominent peak in the observed recoil energy around $E_{\text{obs}} \sim 30$ eV. For tungsten carbide the energy loss curve is sharp for tungsten nuclei but smooth for carbon nuclei. However, due to the A^2 factor in (1), the DM recoil rate in tungsten carbide is completely dominated by tungsten recoils, and therefore the sharp threshold results in a prominent peak feature. Because of the heavy nuclear mass of tungsten, the peak is only visible for DM mass above 1 GeV. Figure 5 shows the differential event rate in WC for 1 GeV and 5 GeV DM particles, and a clear peak is visible in the latter. As discussed in [15], the presence or absence of the peak in the observed recoil spectrum could be used to determine if the observed events are indeed due to nuclear recoils. For this purpose it is important that the peak is not masked by other processes, such as, e.g., electronic/trigger noise that may dominate the event rate at very low energies. In this view, the very high displacement threshold energy of tungsten is interesting, as it results in the peak centered at ~ 50 eV, almost twice that of diamond.

Because the peak feature is not expected for electron recoils, it can be used to enhance the signal identification for an electron recoil dominated background. The detailed characterization of this effect will depend on the details of the experimental setup, but to get an idea of the possible gain, we have simulated an electron recoil background following the tritium background component reported in [37] and computed the discovery reach of a diamond detector for a spin-independent DM signal with or without the energy loss effect. To find the discovery reach we perform a likelihood-ratio test of the signal + background model to a background only model for the simulated data, where the signal model is the spin-independent DM spectrum with or without the energy loss. Figure 6 shows the gain, i.e., the ratio of the reach after the energy loss effect to the reach without the effect. For a 100 kg year

experiment we observe a gain of $\mathcal{O}(40\%)$, and for a 1 kg year experiment the gain is $\mathcal{O}(10\%)$.

Although directional trends are not a focus of this study, we have produced plots of the angular distribution of defect creation thresholds in Fig. 7 for the benefit of the reader, with the caveat that, due to the recombination trends shown in Fig. 2, some of these may be dominated by noise. A detailed description of the directional behavior of defect creation and energy loss requires further research.

As a result of the motion of the lab frame with respect to the galactic rest frame, the dark matter recoil rate exhibits a preferred direction. The resulting daily modulation of the low energy event rate due to the ionization threshold in ionization-based detectors has been studied in [20,36,38]. Due to the strong directional dependence of the energy loss in the crystal, one might wonder if a daily modulation effect should also appear in the peak feature shown in Fig. 5. However, for the peak to appear in the spectrum, the DM particle must be heavy enough to excite recoils well above the defect creation threshold. As described in [36], the angular recoil spectrum is then broad, so the effect of the directional variation in the energy loss gets effectively averaged over, and there is no noticeable daily modulation in this effect.

IV. CONCLUSIONS

We have performed molecular dynamics simulations to determine the amount of energy lost in lattice deformations in low energy nuclear recoil events as a function of the recoil direction and energy. We have described how this effect modifies the observed recoil spectrum in phonon-based detectors. Some materials, most notably diamond, exhibit a sharp defect creation threshold, and for those materials the energy loss effect results in a prominent peak in the observed recoil spectrum. Via simulations of a number of materials with different physical properties, we have demonstrated a large variability in the profile of the energy loss and of the recoil spectrum.

In [15] we have discussed how the energy loss features can be used to determine whether the observed low energy excess event rate [10] is due to nuclear recoils. In this paper we have shown how the expected DM recoil rate changes as a result of the energy loss and depending on the target material, under the standard assumptions of a spin-independent interaction and standard halo model. It is evident from the results shown above that an ideal target material for observation of this effect is hard, with a simple crystal structure, and low propensity for damage recombination. Of the materials we have simulated, the most promising candidates are diamond at low recoil energies and tungsten carbide at slightly higher recoil energies. The simulated results in this paper can be experimentally validated using a low energy neutron beam wherein a monoenergetic neutron beam scatters off the detector and the recoil energy is

measured using the scattering angle and/or time of flight like TUNL.¹

The energy loss data described in this work can be found in an online repository,² and we plan to add data for other detector materials in the future. In future work we shall also investigate how the peak feature is affected by relaxing the

assumptions on the spin-independent interaction or on the DM halo model.

ACKNOWLEDGMENTS

The authors wish to thank the Finnish Computing Competence Infrastructure (FCCI) for supporting this project with computational and data storage resources. Financial support from Academy of Finland, Project No. 342777, is gratefully acknowledged.

¹<https://tunl.duke.edu>.

²<https://github.com/sebsassi/elosssim>.

-
- [1] N. Aghanim *et al.*, Planck 2018 results. VI. Cosmological parameters, *Astron. Astrophys.* **641**, A6 (2020); Erratum, *Astron. Astrophys.* **652**, C4 (2021).
- [2] G. Bertone, D. Hooper, and J. Silk, Particle dark matter: Evidence, candidates and constraints, *Phys. Rep.* **405**, 279 (2005).
- [3] E. Aprile *et al.*, Dark Matter Search Results from a One Ton-Year Exposure of XENON1T, *Phys. Rev. Lett.* **121**, 111302 (2018).
- [4] C. W. Fink *et al.*, Performance of a large area photon detector for rare event search applications, *Appl. Phys. Lett.* **118**, 022601 (2021).
- [5] A. H. Abdelhameed *et al.*, First results from the CRESST-III low-mass dark matter program, *Phys. Rev. D* **100**, 102002 (2019).
- [6] A. Aguilar-Arevalo *et al.*, Results on Low-Mass Weakly Interacting Massive Particles from a 11 kg-Day Target Exposure of DAMIC at SNOLAB, *Phys. Rev. Lett.* **125**, 241803 (2020).
- [7] E. Armengaud *et al.*, Searching for low-mass dark matter particles with a massive Ge bolometer operated above-ground, *Phys. Rev. D* **99**, 082003 (2019).
- [8] R. Strauss *et al.*, Gram-scale cryogenic calorimeters for rare-event searches, *Phys. Rev. D* **96**, 022009 (2017).
- [9] R. Agnese *et al.*, Nuclear-recoil energy scale in CDMS II silicon dark-matter detectors, *Nucl. Instrum. Methods Phys. Res., Sect. A* **905**, 71 (2018).
- [10] A. Fuss, M. Kaznacheeva, F. Reindl, and F. Wagner, EXCESS workshop: Descriptions of rising low-energy spectra, *SciPost Phys. Proc.* **9**, 001 (2022).
- [11] Y. Kahn and T. Lin, Searches for light dark matter using condensed matter systems, *Rep. Prog. Phys.* **85**, 066901 (2022).
- [12] A. Mitridate, T. Trickle, Z. Zhang, and K. M. Zurek, Snowmass white paper: Light dark matter direct detection at the interface with condensed matter physics, [arXiv:2203.07492](https://arxiv.org/abs/2203.07492).
- [13] B. Campbell-Deem, S. Knapen, T. Lin, and E. Villarama, Dark matter direct detection from the single phonon to the nuclear recoil regime, *Phys. Rev. D* **106**, 036019 (2022).
- [14] F. Kadribasic, N. Mirabolfathi, K. Nordlund, and F. Djurabekova, Crystal defects: A portal to dark matter detection, [arXiv:2002.03525](https://arxiv.org/abs/2002.03525).
- [15] M. Heikinheimo, S. Sassi, K. Nordlund, K. Tuominen, and N. Mirabolfathi, Identification of the low energy excess in dark matter searches with crystal defects, [arXiv:2112.14495](https://arxiv.org/abs/2112.14495).
- [16] A. P. Thompson, H. M. Aktulga, R. Berger, D. S. Bolintineanu, W. M. Brown, S. Crozier, P. in 't Veld, A. Kohlmeyer, S. G. Moore, T. D. Nguyen, R. Shan, M. J. Stevens, J. Tranchida, C. Trott, and S. J. Plimpton, LAMMPS—A flexible simulation tool for particle-based materials modeling at the atomic, meso, and continuum scales, *Comput. Phys. Commun.* **271**, 108171 (2022).
- [17] K. Nordlund, M. Ghaly, R. S. Averback, M. Caturla, T. Diaz de la Rubia, and J. Tarus, Defect production in collision cascades in elemental semiconductors and FCC metals, *Phys. Rev. B* **57**, 7556 (1998).
- [18] PARCAS computer code, available open source at <https://gitlab.com/acclab/parcas/>.
- [19] M.-J. Caturla, T. Diaz de la Rubia, and G. H. Gilmer, Point defect production, geometry and stability in silicon: A molecular dynamics simulation study, *Mater. Res. Soc. Symp. Proc.* **316**, 141 (1994).
- [20] F. Kadribasic, N. Mirabolfathi, K. Nordlund, A. E. Sand, E. Holmström, and F. Djurabekova, Directional Sensitivity in Light-Mass Dark Matter Searches with Single-Electron Resolution Ionization Detectors, *Phys. Rev. Lett.* **120**, 111301 (2018).
- [21] K. Nordlund, Molecular dynamics simulation of ion ranges in the 1–100 keV energy range, *Comput. Mater. Sci.* **3**, 448 (1995).
- [22] P. Vashishta, R. K. Kalia, A. Nakano, and J. P. Rino, Interaction potentials for alumina and molecular dynamics simulations of amorphous and liquid alumina, *J. Appl. Phys.* **103**, 083504 (2008).
- [23] F. Gao and W. J. Weber, Empirical potential approach for defect properties in 3C-SiC, *Nucl. Instrum. Methods Phys. Res., Sect. B* **191**, 504 (2002).
- [24] N. Juslin, Erhart, Träskelin, J. Nord, K. O. E. Henriksson, K. Nordlund, E. Salonen, and K. Albe, Analytical interatomic potential for modeling nonequilibrium processes in the W–C–H system, *J. Appl. Phys.* **98**, 123520 (2005).
- [25] P. Erhart and K. Albe, Analytical potential for atomistic simulations of silicon, carbon and silicon carbide, *Phys. Rev. B* **71**, 035211 (2004).

- [26] F. H. Stillinger and T. A. Weber, Computer simulation of local order in condensed phases of silicon, *Phys. Rev. B* **31**, 5262 (1985).
- [27] J. Tersoff, Modeling solid-state chemistry: Interatomic potentials for multicomponent systems, *Phys. Rev. B* **39**, 5566 (1989); **41**, 3248 (1990).
- [28] K. Nordlund, J. Keinonen, and T. Mattila, Formation of Ion Irradiation-Induced Small-Scale Defects on Graphite Surfaces, *Phys. Rev. Lett.* **77**, 699 (1996).
- [29] P. M. Derlet, D. Nguyen-Manh, and S. L. Dudarev, Multiscale modeling of crowdion and vacancy defects in body-centered-cubic transition metals, *Phys. Rev. B* **76**, 054107 (2007).
- [30] C. Björkas, K. Nordlund, and S. Dudarev, Modelling radiation effects using the ab-initio based tungsten and vanadium potentials, *Nucl. Instrum. Methods Phys. Res., Sect. B* **267**, 3204 (2008); Erratum, *Nucl. Instrum. Methods Phys. Res., Sect. B* **268**, 1529 (2010).
- [31] N. W. Ashcroft and N. D. Mermin, *Solid State Physics* (Saunders College, Philadelphia, 1976).
- [32] T. Diaz de la Rubia, R. S. Averback, R. Benedek, and W. E. King, Role of Thermal Spikes in Energetic Collision Cascades, *Phys. Rev. Lett.* **59**, 1930 (1987); Erratum, *Phys. Rev. Lett.* **60**, 76 (1988).
- [33] K. Nordlund, S. J. Zinkle, A. E. Sand, F. Granberg, R. S. Averback, R. Stoller, T. Suzudo, L. Malerba, F. Banhart, W. J. Weber, F. Willaime, S. Dudarev, and D. Simeone, Primary radiation damage: A review of current understanding and models, *J. Nucl. Mater.* **512**, 450 (2018).
- [34] M.-C. Marinica, F. Willaime, and J.-P. Crocombette, Irradiation-Induced Formation of Nanocrystallites with C15 Laves Phase Structure in bcc Iron, *Phys. Rev. Lett.* **108**, 025501 (2012).
- [35] Y.-N. Liu, T. Ahlgren, L. Bukonte, K. Nordlund, X. Shu, Y. Yu, X.-C. Li, and G.-H. Lu, Mechanism of vacancy formation induced by hydrogen in tungsten, *AIP Adv.* **3**, 122111 (2013).
- [36] M. Heikinheimo, K. Nordlund, K. Tuominen, and N. Mirabolfathi, Velocity dependent dark matter interactions in single-electron resolution semiconductor detectors with directional sensitivity, *Phys. Rev. D* **99**, 103018 (2019).
- [37] R. Agnese *et al.*, Projected sensitivity of the SuperCDMS SNOLAB experiment, *Phys. Rev. D* **95**, 082002 (2017).
- [38] S. Sassi, A. Dinmohammadi, M. Heikinheimo, N. Mirabolfathi, K. Nordlund, H. Safari, and K. Tuominen, Solar neutrinos and dark matter detection with diurnal modulation, *Phys. Rev. D* **104**, 063037 (2021).